PHYSICAL REVIEW E VOLUME 61, NUMBER 1 JANUARY 2000

Dynamics of a penta-hepta defect in a hexagonal pattern

Tammy Tam, Darrick Ohata, and Mingming Wu
Department of Physics, Occidental College, Los Angeles, California 90041
(Received 13 September 1999)

The structure and dynamics of a penta-hepta defect in a hexagonal pattern are studied experimentally. The hexagonal pattern is formed by placing a layer of soap bubbles (diameter ~1 mm) on a flat glass plate. We find that an isolated penta-hepta defect in a bubble raft with free boundary always moves along the direction perpendicular to the wave vector of the nonsingular mode and towards the nearest boundary. The structure of the penta-hepta defect is found to be similar to that found in nonequilibrium pattern forming systems.

PACS number(s): 47.54.+r, 61.72.−y, 47.55.Dz

This Rapid Communication describes experimental investigations on the structure and dynamics of an isolated penta-hepta defect in a hexagonal pattern formed by a layer of equal sized (diameter ~1mm) soap bubbles. Soap bubbles in a certain size range are known to ''crystallize'' spontaneously on a flat surface and form a perfect hexagonal pattern [1]. Previous experimental and theoretical work demonstrated that such a soap bubble raft possesses many of the properties of 2D crystalline systems [1–3]. It has been shown that the interactions between neighboring bubbles is described by a van der Waals or capillary attraction and a short-range or ''overlap'' repulsion [3]. The resulting potential-distance curve reaches a minimum when the distance between two neighboring bubbles equals the bubble diameter. That is, the hexagonal lattice formed by soap bubbles corresponds to the minimum energy state. Several experiments have demonstrated that properties of dislocations, grain boundaries, and stress-strain curves that are typical to a 2D crystalline system exist in soap bubble raft [1,3].

Recently, attention has been focused on the structure and dynamics of defects in pattern forming systems far from equilibrium, specifically in Rayleigh-Bénard convections [4–13]. It is found that defects play important roles in the wave vector selection of these systems. The defect that most commonly occurred in a 2D hexagonal pattern is the penta-hepta defect (PHD); a pair of a pentagonal and a heptagonal cell instead of two neighboring hexagonal cells. Experimental [5,6] and theoretical [10] work on the structure of PHD has revealed that a PHD requires that two of the three superimposed roll patterns of the hexagonal pattern have dislocations with opposite phase winding numbers. Later observations of the motion of the PHDs in a Rayleigh-Bénard convection [7,8] have inspired a series of theoretical work on the dynamics of the PHDs using the three coupled Ginzburg-Landau equations [11–13]. The mobility of an isolated PHD in a nonoptimal wave vector hexagonal pattern is calculated and the interactions of two PHDs are considered.

It needs to be noted that the hexagonal patterns formed by soap bubbles belong to an *equilibrium* system, while those observed in Rayleigh-Bénard convection belong to a *nonequilibrium* system. However, both systems are potential systems [3,10]. We hope that results presented here will provide insights for the studies of the motion of defects in nonequilibrium systems. Furthermore, it will stimulate theoretical work on the structure and dynamics of defects in 2D crystalline systems.

The experiment requires a very simple laboratory setup. Soap bubbles are generated with a hypodermic needle submerged in a soap solution. The needle is supplied with nitrogen at a constant pressure provided by an assembly of a pressure needle valve, a pressure regulator, and a compressed nitrogen gas tank. The size of the nitrogen filled soap bubbles is adjusted by the needle size and the pressure of the nitrogen. A typical soap solution consists of 28% by weight doubly deionized and distilled water, 44% regent grade glycerine, and 28% Miracle Bubbles (Imperial Toy Corporation, Los Angeles). The bubbles first float on the surface of the soap solution and form naturally a perfect hexagonal pattern. They are then transferred to a flat glass plate with a plastic spoon. Each transfer contains about a dozen bubbles and a small amount of solution. When the bubbles of the first transfer are placed on the glass plate, they form a perfect hexagonal patch naturally. At each subsequent transfer, the bubbles are added carefully to the edges of the perfect hexagonal patch and the 2D ''crystal'' grows spontaneously. Two different boundary conditions are used in our experiments, one is bounded with a 5.41 cm in diameter plastic ring [Fig. 1(a)] and the other is with free boundary [Fig. 1(b)]. Defects can be seen close to the boundary in the bubble raft with boundary. In the free boundary case, the entire bubble raft is free of defects. The bubbles are very uniform in size, as can be seen by the regularity of the bubble raft in Fig. 1. The hexagonal pattern shown in Fig. 1 is a stable state, it will stay motionless for about an hour. If the raft is left for more than an hour, the bubble size shrinks due to the gas diffusion through the wall. In this case, a void will appear near the boundary.

Since soap bubbles form a perfect hexagonal pattern spontaneouly, it is thus necessary for us to introduce PHDs into the system for the study of defect motion. The procedure for introducing a single defect is as follows. First, a perfect hexagonal patch is made, as shown in Fig. 1. For the data shown below, the size of the cell is between 9.0 to 12 cm^2, approximately half the size of the cell shown in Fig. 1(b). Second, the perfect hexagonal pattern is raked by a wet needle. Multiple defects are created simultaneously of which most of them are PHDs. Third, a single PHD near the center of the cell is isolated by getting rid of the unwanted defects. This is usually done by releasing the stress around the unwanted defects using a wet needle. Occasionally, a single PHD can be created by merging two line defects. Very often,

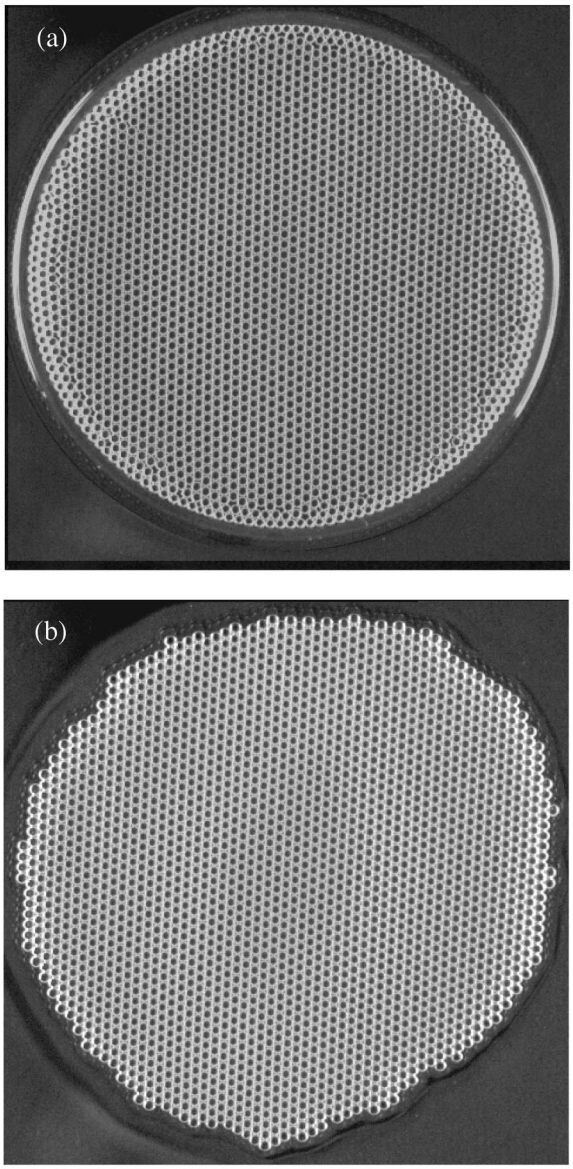

FIG. 1. Perfect hexagonal patterns formed by 0.108 cm in diameter soap bubbles. (a) The bubble raft bounded with a 5.41 cm diameter plastic ring. (b) The bubble raft with free boundary.

we end up with a perfect hexagonal pattern again and the whole process needs to be repeated. In the free boundary case [Fig. 1(b)], the isolated PHD is not stable; it moves immediately to its nearest boundary once it is created. This demonstrates that the bubble raft without constraint prefers to stay in its lowest energy state, which is the perfect hexagonal pattern [3]. In the rigid boundary case [Fig. 1(a)], the isolated PHD near the center of the cell is often motionless at the beginning and eventually moves to the boundary. In one case, the motion of the defect is caused by the interactions of the isolated defect near the center with the defects near the boundary. The motion of the isolated PHD is complicated by the random distribution of the defects around the boundary. In the other case, a void is formed after a few hours of waiting due to the bubble size shrinkage, and the defect always chose to move towards the void in a similar way as in a cell with free boundary. It moves along the direction perpendicular to the wave vector of nonsingular mode. In the following, we focus on studying the motion of a single defect in a hexagonal pattern with *free boundary*.

Images of the cell are recorded for the study of the defect motion using a super VHS recorder (JVC, BRS822DXU). A time series of 30 to 60 images that cover the central portion of the cell is digitized from the video tape for further data analysis. Two consecutive images are 1*s* apart. Figure 2(a) shows a typical image of an isolated PHD. It consists of 256 pixel
$\times$ 256 pixel, which corresponds to a viewing area of 2.13 cm $\times$ 2.13 cm. The bubble size is 0.108 cm. The pair of pentagonal and heptagonal cells are marked with two white bars in Fig. 2(a). Figure 2(b) is the gray scale rendition of the modulus $|A(\mathbf{k})|^2$ of the Fourier transform of $A(\mathbf{x})$, where $A(\mathbf{x})$ is the gray scale of the hexagonal pattern shown in Fig. 2(a). The six dots indicate the locations of the wave vectors $\pm\mathbf{k_1}$, $\pm\mathbf{k_2}$, $\pm\mathbf{k_3}$ of the three superimposed roll patterns. $\mathbf{k_1}$, $\mathbf{k_2}$, and $\mathbf{k_3}$ are oriented 120° with respect to each other counterclockwise, a convention used in previous publications [5,13]. Each roll pattern is reconstructed by performing an inverse fourier transform of $A(\mathbf{k})$ using one pair of peaks. For example, Fig. 2(c1) is obtained by inverse Fourier transforming $A(\mathbf{k})$ after one pair of peaks of $A(\mathbf{k})$ at locations $\pm\mathbf{k_1}$ are singled out using tanh windows [14]. The roll pattern with wave vectors $\pm\mathbf{k_1}$ is defect free [Fig. 2(c1)], while the second and third roll patterns with wave vectors $\pm\mathbf{k_2}$ and $\pm\mathbf{k_3}$ [Fig. 2(c2) and 2(c3)] contain a defect each. A standard demodulation technique is used here to study the structure of the defect [5]. As we know, the gray scale $A(\mathbf{x})$ of a nearly perfect hexagonal pattern can be written as

$$A(\mathbf{x}) = \sum_{j=1}^{3} [\hat{A}_j(\mathbf{x}) e^{i\mathbf{k_j}\cdot\mathbf{x}} + \text{c.c}]. \tag{1}$$

Here $\hat{A}_j(\mathbf{x})(j=1,2,3)$ is the slow varying amplitude of one of the three superimposed roll patterns. These three complex amplitudes contain the essential information about the defect. To obtain $\hat{A}_j(\mathbf{x})$, we first shift the peak of $A(\mathbf{k})$ at $\mathbf{k_j}$ to the origin, and then do a low pass filtering (tanh window) [14] around the origin. The inverse Fourier transform of the filtered $A(\mathbf{k})$ gives us $\hat{A}_j(\mathbf{x})$. The phase of the $\hat{A}_j(\mathbf{x})$ is shown in Figs. 2(d1)–2(d3). No singularity is observed in the phase diagram of the first roll pattern [Fig. 2(d1)], while singularity of topological winding number + or -1 is shown at the core of the defect in the phase diagram of the second or third roll pattern [Figs. 2(d2) and 2(d3)]. The definition of the phase winding number can be found in Refs. [9] and [13]. The modulus $|\hat{A}_j|^2$ of the complex amplitude demonstrates a minimum at the core of the defect for the second and the third roll patterns. Gray scale rendition of $|\hat{A}_2(\mathbf{x})|^2$ is shown in Fig. 2(e). The above shows that the structure of the PHD in a soap bubble raft presents similar characteristics to that observed in Rayleigh-Bénard convections [5,8].

The trajectory of the PHD is shown in Fig. 3 and it is extracted from a time series of 32 images. The *x*-*y* coordinates of the PHDs are determined by locating the positions of the singularities in the phase diagrams such as the one shown in Fig. 2(d2) using Global Lab Image software (Data Translation). As is seen, the positions of the singularities are sharply defined in the phase diagrams [Figs. 2(d2) and 3(d3)]. The error of each measured position is ± 1 pixel,

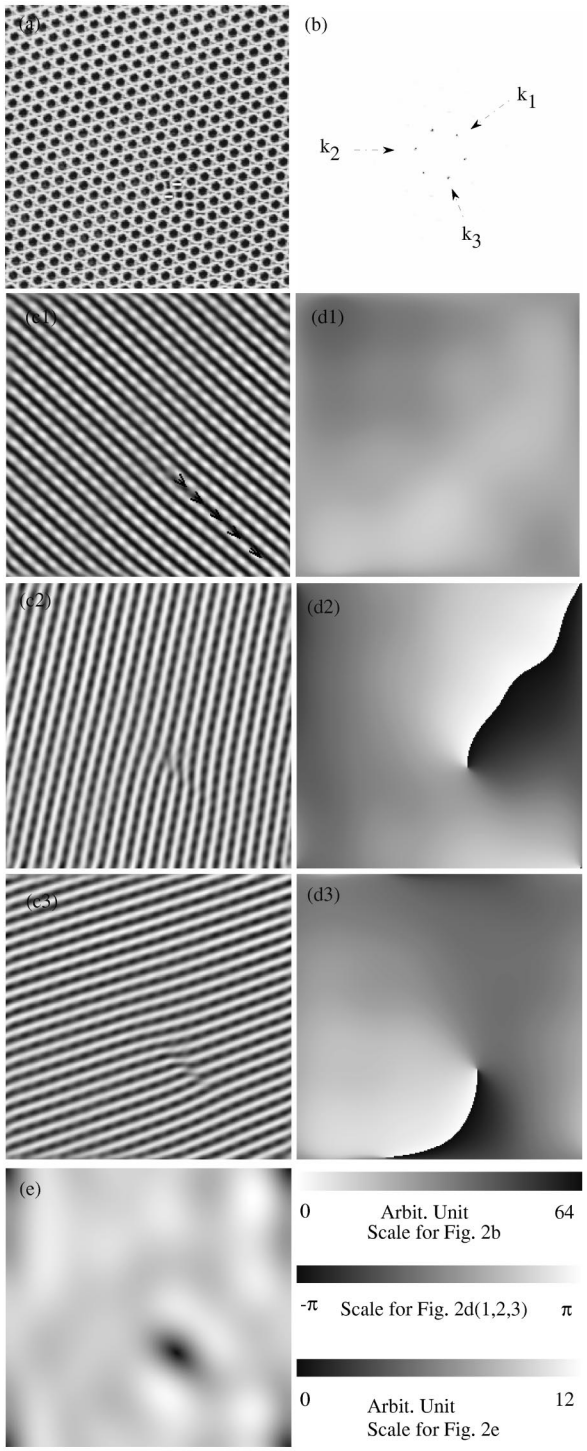

FIG. 2. (a) Hexagonal pattern with an isolated PHD formed by soap bubbles of diameter 0.108 cm. The pair of pentagonal and heptagonal cells are marked with two white bars. (b) Modulus $|A(\mathbf{k})|^2$ of the Fourier transform of the hexagonal pattern [Fig. 2(a)]. Linear gray scale is shown at the lower right corner. Note the inverse gray scale. (c1)–(c3) Three roll patterns with wave vectors $\mathbf{k_1}$, $\mathbf{k_2}$, and $\mathbf{k_3}$. The arrows in (c1) indicate the direction and trajectory of the PHD. The two ends of each arrow are determined by the locations of the defects of $5s$ apart. (d1)–(d3) Gray scale renditions of the phases of the complex amplitudes $\hat{A}_j(\mathbf{x})(j=1,2,3)$. Linear gray scale is shown at the bottom. (e) Gray scale rendition of the square root of $|\hat{A}_2(\mathbf{x})|^2$. Linear gray scale is shown on the right side of the image.

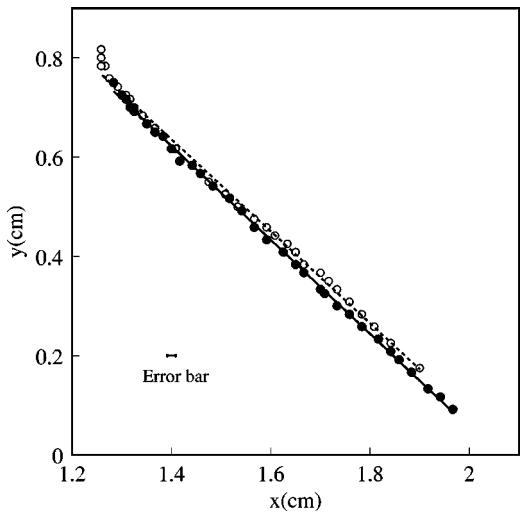

FIG. 3. Trajectory of the PHD. The origin (0,0) of the plot corresponds to the lower left corner of the image. x and y axes are the (x,y) coordinates of the PHD. ○/●. Data points determined using phase diagram of the roll pattern with wave vector $\mathbf{k_2}/\mathbf{k_3}$. Dashed and solid lines are obtained from the linear fit to ○ and ● data points, respectively.

which corresponds to ± 0.0084 cm. The trajectory of the PHD is consistently straight in our experiments. The interesting finding here is that the isolated PHD always moves along the direction perpendicular to the wave vector of the nonsingular mode ($\mathbf{k_1}$ in our experiment) and towards the nearest boundary. In other words, the PHDs always prefer to climb along the defect free rolls. This is more clearly demonstrated by the arrows in Fig. 2(c1), in which the two ends of the arrows are determined by the locations of the PHDs of $5s$ apart. The motion of the defect in the second or the third roll pattern consists of both a glide and a climb motion. Movies of the defect motion can be seen at website http://mwu.phys.oxy.edu/soap-bubble/soap.html. The direction of the trajectory is also determined quantitatively using the slope of the trajectory from a linear fit to the data in Fig. 3. The angle between the trajectory and the $+x$ axis is obtained to be $-43.1°$. The direction of the wave vector $\mathbf{k_1}$ is determined using the location of the peak at $\mathbf{k_1}$ in Fig. 2(b), which gives us an angle of 48.4° (between $\mathbf{k_1}$ and the $+x$ axis). The angle between the direction of the trajectory and the wave vector $\mathbf{k_1}$ for this particular run is thus 91.5°. Summarizing the seven experimental runs, we obtain the angle between the wave vector $\mathbf{k_1}$ and the trajectory to be $90.8 \pm 2.0°$.

To investigate the velocity of the PHD, we plot the distance that the PHD has traveled since its creation versus time (Fig. 4). The slope of that gives us the speed of the defect motion. It needs to be noted that the velocity data presented here is taken from images of the central portion of the cell. There is a few seconds duration of transient motion before the PHD reaches a constant speed (as shown in Fig. 4), and it speeds up near the boundary of the cell. In this particular run, the velocity is obtained to be 0.0325 ± 0.005 cm/s. The speed of the PHD is in the range of 0.0141–0.0330 cm/s for the seven experimental runs mentioned above. The range of the speed could be due to the slight variations of the thickness of the fluid layer underneath the bubbles. We found qualitatively that the PHD moves faster when the layer is thicker;

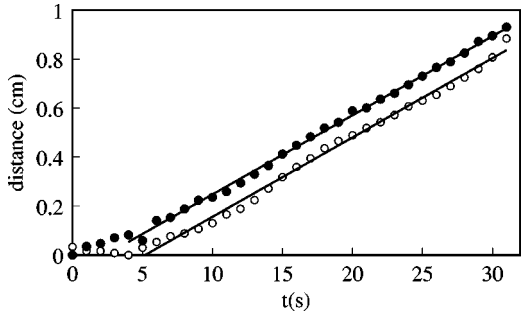

FIG. 4. Distance of the PHD from its starting point vs time. ○/●, Data points determined using the phase diagram of the roll pattern with wave vector $\mathbf{k_2}/\mathbf{k_3}$. Solid lines are obtained from linear fits to the experimental data.

however, the current experimental setting does not allow us to change the layer thickness quantitatively. Cautions have been taken to keep the layer thickness a constant from one run to the other. A new apparatus is being contemplated for further quantitative study of the speed of the PHD.

A full theoretical explanation of the experimental results presented above is still lacking. Here, we would like to address two issues that are pertinent to the problem. First, what is the driving force behind the PHD motion? Theoretical work on nonequilibrium systems using the coupled Ginzburg-Landau (GL) equations [12] has demonstrated that the driving force can be the Peach-Köhler force, which is due to the deviation of the wave vector from its optimal value. The GL theory finds that an isolated PHD moves *parallel* to the wave vector of nonsingular mode in a system where $\mathbf{k_2}$ and $\mathbf{k_3}$ are equal in magnitude and nonoptimal. If $\mathbf{k_2}$ and $\mathbf{k_3}$ are optimal, the PHD stays put. These results differ from our finding that the PHD always moves *perpendicular* to the wave vector of nonsingular mode. In our experiments, the magnitudes of $\mathbf{k_2}$ and $\mathbf{k_3}$ are equal in some of the runs and differ less than 5% in others. This suggests that the GL theory does not apply to our system and the driving force of the PHD motion comes from other sources. Now, the fact that a PHD leaves the bubble raft spontaneously suggests that there is a free energy associated with it, that work must be done to move the PHD into a perfect hexagonal pattern. This indicates that the driving force can be the potential force (elastic force, for instance) associated with the free energy of the system, and it takes a minimum amount of work for the defect to climb along the defect free rolls. The direction of the PHD motion is further finalized by the boundary. The PHD always moves towards the nearest boundary. The second issue concerns the effect of viscous force on the speed of the PHD. We found that the PHD moves faster in a bubble raft with a thicker fluid layer underneath the bubbles. It is reasonable to suggest that the free energy of the system should include contributions from both the elastic force of the bubble raft and the viscous force due to the fluid layer underneath.

To summarize, we find that (i) an isolated PHD moves along the direction perpendicular to the wave vector of the nonsingular mode and towards the nearest boundary in a cell with free boundary; (i) an isolated PHD stays motionless in a cell with rigid boundary.

The authors would like to thank Professor Guenter Ahlers for insightful discussions on the subject. M. Wu would like to thank Dr. Tsimring on various email communications, especially on the theoretical explanations of the results presented above. This work is supported by the Petroleum Research Fund (Grant No. ACS-PRF# 32904-GB9) and the Research Corporation (Contract No. CC4612).

[1] L. Bragg, J. Sci. Instrum. **19**, 148 (1942).
[2] L. Bragg and J. F. Nye, Proc. R. Soc. London, Ser. A **190**, 474 (1947).
[3] M. M. Nicolson, Proc. Cambridge Philos. Soc. **45**, 288 (1948).
[4] V. Croquette, Contemp. Phys. **30**, 153 (1989).
[5] S. Ciliberto, P. Coullet, J. Lega, E. Pampaloni, and C. Perez-Garcia, Phys. Rev. Lett. **65**, 2370 (1990).
[6] S. Ciliberto, E. Pampaloni, and C. Perez-Garcia, J. Stat. Phys. **64**, 1045 (1991).
[7] J. de Bruyn, E. Bodenschatz, S. Morris, S. Trainoff, Y. Hou, D. Cannell, and G. Ahlers, Rev. Sci. Instrum. **67**, 2043 (1996).
[8] E. Bodenschatz, W. Pesch, and G. Ahlers, Annu. Rev. Fluid Mech. (to be published).
[9] M. Cross and P. Hohenberg, Rev. Mod. Phys. **65**, 898 (1993).
[10] L. M. Pismen and A. A. Nepomnyashchy, Europhys. Lett. **24**, 461 (1993).
[11] M. I. Rabinovich and L. S. Tsimring, Phys. Rev. E **49**, R35 (1994).
[12] Lev S. Tsimring, Phys. Rev. Lett. **74**, 4201 (1995).
[13] Lev S. Tsimring, Physica D **89**, 368 (1996).
[14] A function $0.25[\tanh(r+4)/10+1][\tanh(4-r)/10+1]$ is used to multiply $A(\mathbf{k})$, where r is the distance to the peak $\mathbf{k}_j$. The function has a hat shape that centers around $r=0$, the top width is 4 and bottom width is 10.